A Pendulum Target Balance for Ion Engine Thrust Measurement

IEPC-2007-149

Presented at the 30th International Electric Propulsion Conference, Florence, Italy
September 17-20, 2007

Paolo Gessini*, Gilberto Marrega Sandonato†, Ricardo Toshiyuki Irita‡, José Américo Neves Gonçalves§ and George Favale e Fernandes**
Instituto Nacional de Pesquisas Espaciais (INPE), São José dos Campos, SP, 12227-010, Brazil

Abstract: A thrust measurement system, based on a Pendulum Target Balance (PTB) is being built in order to characterize the performance of the ion thrusters developed at the Brazilian National Institute for Space Research (INPE). A theoretical analysis of the system is presented, together with the results of a first prototype calibration, in good agreement with numerical simulations. A final model is being assembled and will be optimized and calibrated to be capable of thrust measurements with a resolution in the μN range.

Nomenclature

D	=	distance from center of gravity to calibration mass
f	=	focal length
F	=	thrust
g	=	acceleration of gravity at sea level
I	=	PTB moment of inertia with respect to suspension axis
m	=	PTB mass
m_C	=	calibration mass
M_F	=	thrust moment
M_W	=	weight moment
MAG	=	optical system magnification
OVL	=	optical system overall length
P	=	optical path length
R	=	distance from center of gravity to suspension axis
R'	=	distance from thrust axis to suspension axis
w	=	laser beam radius
w_0	=	laser beam waist radius
W	=	weight
z	=	laser beam propagation distance
λ	=	wavelength
μ	=	additional mass moment of inertia with respect to suspension axis
v	=	oscillation frequency

* Postdoctoral Research Fellow, Associated Plasma Laboratory (LAP), paolo@plasma.inpe.br.
† Senior Researcher – Head of EP Group, Associated Plasma Laboratory (LAP), gms@plasma.inpe.br.
‡ Senior Researcher, Associated Plasma Laboratory (LAP), irita@plasma.inpe.br.
§ Senior Researcher, Associated Plasma Laboratory (LAP), americo@plasma.inpe.br.
** Graduate Student, Associated Plasma Laboratory (LAP), georgeff@plasma.inpe.br.

θ = oscillation angle
θ_{FF} = half-angle laser beam divergence
$\Delta\theta$ = rotation
$\Delta\theta_C$ = calibration rotation
Δx = linear displacement

I. Introduction

THE various methods for the measurement of thrust fall into two general categories. Direct methods, where the thruster is suspended on a thrust balance, the displacement of which is measured by a sensor, and indirect methods, where the thruster is fixed and the displacement of a target balance, which is impacted by the thruster exhaust, is measured.

These latter techniques present several advantages over direct methods. The sensitivity of the balance is inversely proportional to the weight of the moving part and, if the thruster is mounted on it, this may be quite heavy. In addition to limiting the instrument sensitivity, this also causes frictional losses due to the suspension. Unless the whole propulsion system is mounted on the balance, as could be the case with an Ablative Pulsed Plasma Thruster (APPT)[1,2], electric power cables, propellant feed lines and, possibly, cooling flow lines will cause a high motion resistance[3,4]. Target systems are currently being used by other investigators for the measurement of momentum and heat fluxes in plasma environments[5].

In general, an indirect system is independent of the specific thruster configuration and allows the measurement of the performance of different propulsion systems without changes to the balance and consequent recalibration[4]. A potential interpretation problem is caused by the imperfect knowledge of the interaction processes between the target and the plume/beam. Problems concern the degree to which momentum is transferred to the target and the angular reflection processes. Impacts, in general, will neither be completely elastic nor inelastic. Another possible problem, with electric thrusters, is ion sputtering. Although this might not be too significant at energy levels below 100 eV, for which not much information is available[6], they definitely become important in ion thruster beams, with kV-level accelerating potentials. Common metals like iron, copper and aluminum have comparable yield factors, while refractory metals, like molybdenum, have considerably lower (roughly 50%) ion-induced sputtering yields and graphite shows the best behaviour[6,7,8]. A possible way to address these problems and reduce the ensuing errors is to use different types of surface finish and different materials. Experiments could be also devised to estimate particle reflection from the target.

The surface conditions, like roughness and sputtering deposits, will affect the interaction between impinging particles and target. This can be described in terms of the accommodation coefficients of various properties. The concept of accommodation coefficient was introduced by Cercignani and Lampis[9]. Simply stated, it quantifies the extent to which a reflected property approximates diffuse reflection. Therefore, the coefficients for tangential momentum and the normal component of translational energy are both 1 or 0, respectively, for completely diffuse or specular, perfectly elastic reflection, as described by the basic Maxwell model[10]. Equilibrium diffuse reflection requires that both the surface temperature and the temperature associated with the reflected gas Maxwellian distribution be equal to the incident gas temperature. This equilibrium between gas and surface is not always satisfied, which means that the thermal accommodation coefficient, indicating to what extent the reflected particles have their temperature adjusted toward that of the surface, will be less than unity. While the interaction between "engineering" surfaces and gases at normal temperature, in general, approximates diffuse reflection with complete thermal accommodation, there are cases when this assumption should be critically reviewed. These include smooth metal surfaces that have been outgassed, impacts of particles with molecular weight much smaller than that of the surface molecules or with translational energy, relative to the surface, larger than several electron volts[11]. Lord has extended the Cercignani-Lampis model to include the case of diffuse reflection with incomplete thermal accommodation, the most common and useful generalization[12]. From what stated above, this should approximate well the interaction between the ion thruster beam and our target, especially as the surfaces get sputtered and contaminated during the course of the various experimental runs.

At the very least, an indirect system should be good for comparative tests, if we can assume the surface accommodation coefficients to have an approximately constant, though not exactly known, value. The presence in the plume of particles rebounding from the target with an appreciable axial momentum (up to the limiting case of elastic collisions, with accommodation coefficients equal to zero) will lead to overestimating the thrust. As, in general, accommodation coefficients are a function of the surface roughness, cleanliness, temperature and of the

impinging particle molecular weight and kinetic energy[11], our assumption might not be rigorously verified throughout an experimental campaign. This will cause an error even in the relative measurement.

Our imperfect knowledge of the accommodation coefficients and the fact that they might vary appreciably with the target use and the discharge conditions is the main concern when using a target thrust measurement system. If appropriate steps are taken, though, to reduce the uncertainty in the measurements, as in the type of target described in this paper, the advantages discussed above may make the use of an indirect system preferable over a direct one.

II. The Measurement System

The thrust measurement system developed in-house at the Associated Plasma laboratory (LAP) of the Brazilian National Institute for Space Research (INPE) consists of a Pendulum Target Balance (PTB), a Laser Optical Lever (LOL) and a Position Sensitive Detector (PSD).

A. The Pendulum Target Balance (PTB)

The thrust balance designed to perform measurements at INPE is, essentially, a physical pendulum, mounted and oscillating with negligible friction on simple knife-edge suspensions. The actual blades may need to be periodically replaced as they wear out. As an alternative, hard polished metal rollers on a flat polished surface may be substituted for the knife-edges, thus reducing the wear to an inappreciable minimum. The axis of suspension would then be at the centre of the roller and not at the knife edge any longer, the radius of curvature perfectly definite and constant[13]. The whole device presents a plane of symmetry normal to the suspension axis and therefore lends itself to a two-dimensional analysis. Fig. 1 shows a schematic of the PTB, quite different from the actual device, as can be seen in Figs. XXX. This corresponds to an initial design idea and was maintained as it shows more clearly the various parts and dimensions involved, quite difficult to see in the final design.

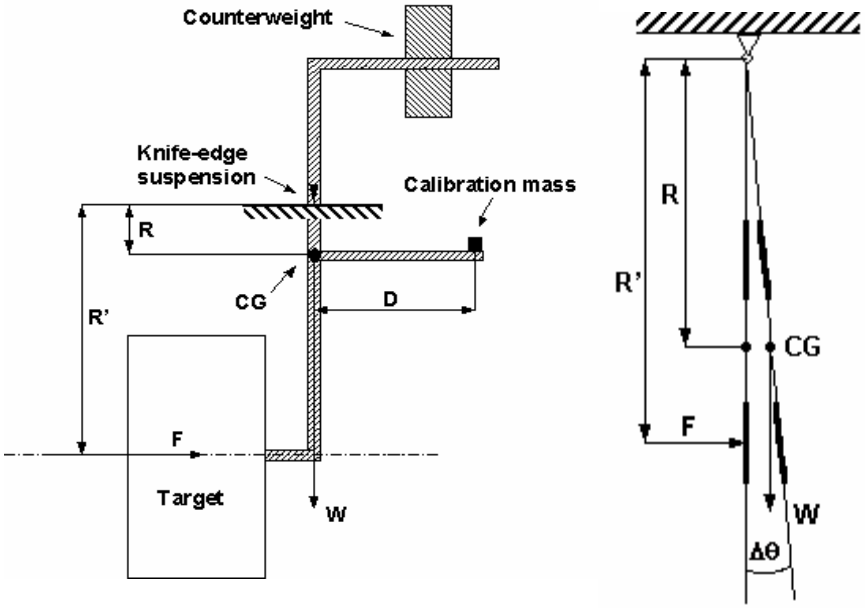

Figure 1. The Pendulum Target Balance (PTB) and its operation (right).

Assuming the thruster plume to be axisymmetric and the target accurately positioned, we can consider the momentum transferred from the plume as equivalent to a force (thrust) F acting along the target axis of symmetry, at a distance R' from the suspension axis. By adjusting the positions and the masses of the counterweights, we can ensure that the PTB is vertical in its equilibrium position and vary the distance R between the center of gravity (CG) and the suspension axis. Provided the former is lower than the latter, this equilibrium position will be stable.

When the thruster plume impinges on the target, the PTB moves and reaches a new equilibrium position after a transient, or just oscillates about the old one, depending on whether the thrust is continuous or impulsive. For small movements, the plume interception will not vary substantially and we can assume the momentum transfer to be equivalent to a moment

$$M_F = FR', \tag{1}$$

The weight W generates a moment

$$M_W = mgR\sin\theta\ , \tag{2}$$

opposing that of F, where m is the mass of the PTB and θ the amplitude of the oscillation. For small oscillations, this reduces to

$$M_W = mgR\,\theta\ , \tag{3}$$

The equation describing the motion of our PTB can thus be written as[14]

$$I\ddot{\theta} = \left(M_F - M_W\right) = \left(FR' - mgR\,\theta\right) \tag{4}$$

where I is the moment of inertia of our PTB with respect to the suspension axis. For the case of a continuously applied thrust F, the equilibrium position rotation, from a simple balance of moments, is

$$\Delta\theta = \frac{F}{mg}\left(\frac{R'}{R}\right) = \frac{M_F}{mgR}\ . \tag{5}$$

The mass m can be accurately determined by weighting the PTB. An accurate determination of R and I is not so trivial. The PTB frequency ν is, for small oscillations,

$$\nu = \frac{1}{2\pi}\sqrt{\frac{mgR}{I}}\ . \tag{6}$$

This can be determined with great accuracy, in a low-damping system as our PTB, by simply counting the number of oscillations in an appropriately long period of time. R could actually be determined experimentally by balancing the PTB to find the position of its CG and I could then be calculated. An alternative route is to determine I according to

$$I = \mu\frac{\nu^2}{\nu'^2 - \nu^2}\ . \tag{7}$$

which is an application of the Huygens theorem[14], and then calculate R. In Eq. (2.7), μ is the moment of inertia with respect to the suspension axis of an additional mass, symmetric with respect to such axis, and ν' is the PTB small oscillation frequency after the addition of such a mass. As μ is precisely known and the frequencies can be accurately measured, I can be determined with very little error and R subsequently calculated.

A straightforward direct calibration of the PTB can be performed by means of a calibration mass m_C, positioned at a distance D from CG such that, under the effect of gravity, it will produce a calibration moment

$$M_C = m_C gD\ . \tag{8}$$

If the calibration arm is at the CG position, the addition of the calibration mass does not change the distance R, but only moves the position of CG "aft", causing a rotation of the PTB given by

$$\Delta\theta_C = -\frac{m_C}{m}\left(\frac{D}{R}\right) = -\frac{M_C}{mgR}\ , \tag{9}$$

taken as negative because it opposes the rotation given by the thruster plume impingement. If the calibration arm is not at the CG position, as long as $m_C << m$ the error given by the variation in R will be negligible.

From Eqs. (2.9) and (2.5) we obtain, for the PTB sensitivity, the expression:

$$\frac{F}{\Delta\theta} = \frac{m_C g}{\Delta\theta_C}\left(\frac{D}{R'}\right), \tag{10}$$

where all the quantities on the RHS are known or can be immediately measured.

The calibration can be performed inside the chamber, with the PTB mounted in the same way as that used during the thrust measurements. For the sake of quickness and ease of operation, though, it will be carried out first outside and then inside, but with the chamber open and the thruster off ("cold" calibration). In order to estimate the magnitude of possible effects of the interaction of the thruster plume with the PTB, it would be useful to perform thrust measurements with and without some calibration masses on the PTB. If such effects, for example thermal in nature, are negligible, the balance deflection with a calibration mass on ("hot" calibration) will be sensibly equal to that measured without calibration mass minus that measured with that same mass and no thrust during the "cold" calibration. As the accuracy of such calibration is only affected by errors in the weighting of the masses and the measuring of the distances, the whole procedure is extremely reliable. Measurements with calibration masses on the PTB will be perforce carried out in the course of experimental runs different from those without masses. As the thrust produced in the same operating conditions may exhibit significant variations, it will be necessary to perform several experimental runs in order for the results to be statistically valid.

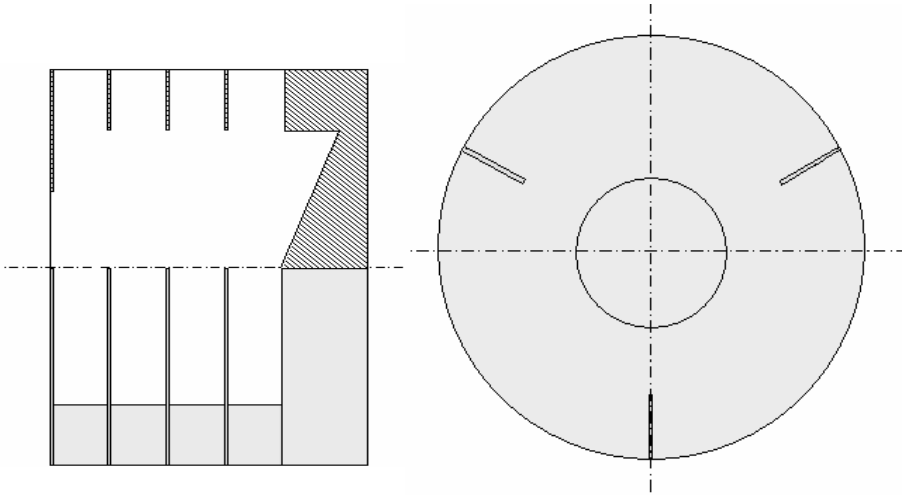

Figure 2. The Cylindrical Target: side view and section, front view (right).

In order to decrease the uncertainty in the measurements due to the imperfectly known plume momentum transfer modalities, the design of the actual target (see Fig. 2) is based on the "cylindrical target" developed by Yanagi and Kimura at the University of Tokyo[15,16] and successfully employed by Japanese investigators. The target consists of a series of discs connected to a back plate. The front disc presents a hole much smaller than the successive ones. The device is positioned in such a way that the thruster plume enters through the front hole, with negligible impingement on the outer surface. Depending on the plume divergence, some of the particles may or may not hit the other discs, but the majority will impinge on the back plate, which has a conical shape to maximize dispersion. As the opening area normal to the radial direction is much larger than that normal to the axial direction the particles, rebounding with different trajectories, will hit the discs and, after various collisions, escape with an essentially radial residual momentum.

Note that Fig. 2 is not a finalized design, but only a conceptual sketch. The dimensioning of the various parts will depend on the actual implementation in the vacuum chamber, in order to minimize, for example, the amount of particles impinging on the outer surface of the front disc or escaping

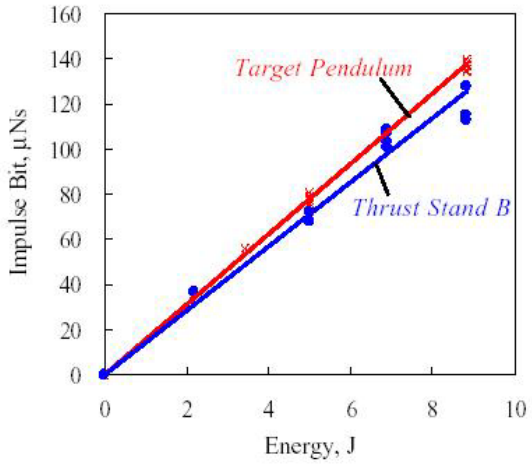

Figure 3. Comparison between thrust stand and target pendulum[19].

with considerable axial momentum from the front aperture. Aluminum, brass and steel, inexpensive and easily machined, and a simple design are used for the initial prototype. Other metals, more resilient to ion sputtering and with better thermo-mechanical characteristics, and an improved design are employed in the final model.

This target design realizes a nearly total transfer of the plume axial momentum to the target, without any assumption about the exact modalities of particle-surface interaction. It therefore allows a measurement of the thrust closely approximating that obtainable with a direct method, but with a much simpler device. A comparison between APPT thrust measurements obtained with the plume impinging on the Japanese cylindrical target and with the thruster mounted on a torsion-type thrust stand shows that the former method, as expected, gives results consistently higher than the latter, due to particles rebounding with a residual axial momentum. This effect, in fact, can never be totally eliminated, but just minimized.

Both methods show a linear dependence of the impulse bit on the discharge energy, as usual in this type of thruster[17,18], with a difference in the slope of only ~10% (see Fig. 3)[19].

B. The Laser Optical Lever (LOL)

The accuracy of our thrust measurement is essentially dependent on the resolution with which we can measure the displacement of the PTB or its rotation. We have decided to measure the rotation with an optical lever. This has the twofold advantage of making the measurement independent of the exact position along the target where it is taken and of being non-intrusive and immune from any kind of interference from the plasma environment.

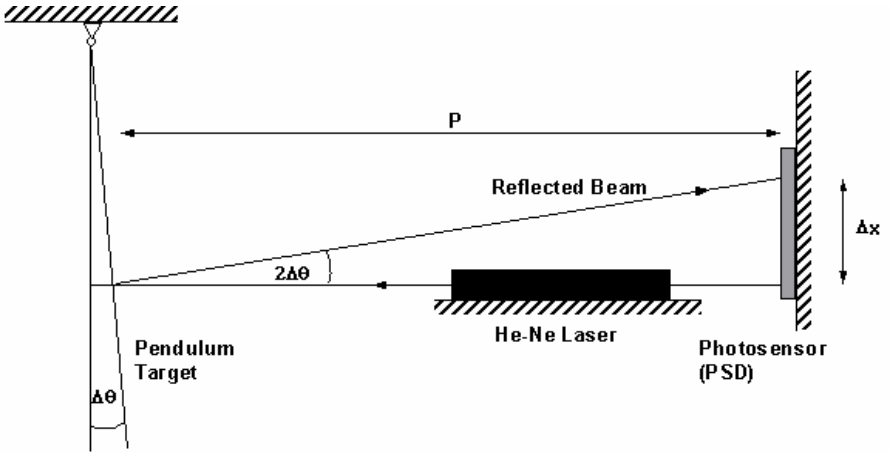

Figure 4. Principle of operation of a LOL.

Optical levers have been long used in many applications. The first light beam deflection galvanometer appeared in 1826. In that year, Poggendorff invented a system to read with great sensitivity the new type of galvanometer just built by Nobili. In these old instruments, a collimated beam of light was reflected off a flat mirror attached to the surface of which the rotation was to be measured. By employing long optical paths, of the order of several meters, the deflection could be easily read as a movement of the end of the beam on a scale. The modern availability of narrow light beams, collimated over long distances, in the form of low-to-medium power lasers, makes this simple instrument even more attractive.

This instrument, used in the measurements described in Ref. 20, will therefore be described as a Laser Optical Lever (LOL). Its principle of operation is illustrated schematically in Fig. 4 for the case $\theta = 0$, where θ is the initial angle between the laser beam and the normal to the target mirror surface. The rotation $\Delta\theta$ is greatly exaggerated for clarity. In reality, the difference between the optical path length P and the distance between the target and the sensor is negligible.

The LOL beam, impinging on a mirror fixed to the back of the pendulum target, translates $\Delta\theta$ into a linear displacement Δx. In general, for $\theta \neq 0$, Δx can be written as

$$\Delta x = P\left[\tan\left(\theta + 2\Delta\theta\right) - \tan\theta\right] \tag{11}$$

which, if $\Delta\theta$ is much smaller than the initial angle θ, reduces, through a first-order Taylor series expansion and the use of trigonometric identities, to

$$\Delta x = 2P\left(1 + \tan^2\theta\right)\Delta\theta \quad . \tag{12}$$

If, in turn, the angle θ is small as well, the above expression further reduces to:

$$\Delta x = 2P\Delta\theta \quad . \tag{13}$$

For $\theta = 10°$, for example, the difference between the value of Δx calculated using Eq. (13) and that calculated using Eq. (12) is only ~3%. Equation (13) also remains accurate in the case of multiple reflections, when a very long optical path is desired in order to increase the sensitivity of the instrument. Now P will be the total optical path length and we can, in general, neglect the corrections due to the particular mirror geometry.

If, instead of reading the laser beam movement on a scale, we want to work with smaller values of P, and therefore use a photo detector to measure small values of Δx, we can still use Eq. (13). If θ happens to be large, Eq. (12) is more appropriate, unless we position the detector perpendicularly to the reflected beam.

One of the main problems while operating with a laser beam is that, in spite of its good collimation, it will spread considerably over long distances. Even if a Gaussian TEM_{00} laser beam wavefront is made perfectly flat at some plane, it will quickly acquire curvature and begin spreading in accordance with[21]

$$w(z) = w_0\sqrt{1+\left(\frac{\lambda z}{\pi w_0^{\,2}}\right)^2} \quad . \tag{14}$$

Here z is the distance propagated from the plane where the wavefront is flat, λ is the wavelength and $w(z)$ is the beam radius after the wave has propagated a distance z.

The beam radius is commonly defined as the radius at which the irradiance (intensity) has fallen to $1/e^2$ (13.5 %) of its peak, or axial, value. At the plane where the wavefront is flat the laser beam is said to have a waist. The beam radius at this location ($z = 0$) is called the waist radius, $w(0) = w_0$. For large values of z, $w(z)$ asymptotically approaches the value

$$w(z) \cong \frac{\lambda z}{\pi w_0} \tag{15}$$

and the $1/e^2$ irradiance contours asymptotically approach a cone of semi-aperture

$$\theta_{FF} = \frac{w(z)}{z} = \frac{\lambda}{\pi w_0} \quad . \tag{16}$$

This value is the half-angle of divergence of the Gaussian TEM_{00} beam.

From Eq. (16) it is clear that, in applications where the optical path is of considerable length, it is advantageous to operate at shorter wavelengths. Also, most He-Ne lasers present an output beam with an extracavity waist, formed by a weak meniscus lens. The beam diameter commonly published in optical catalogues is twice this waist radius.

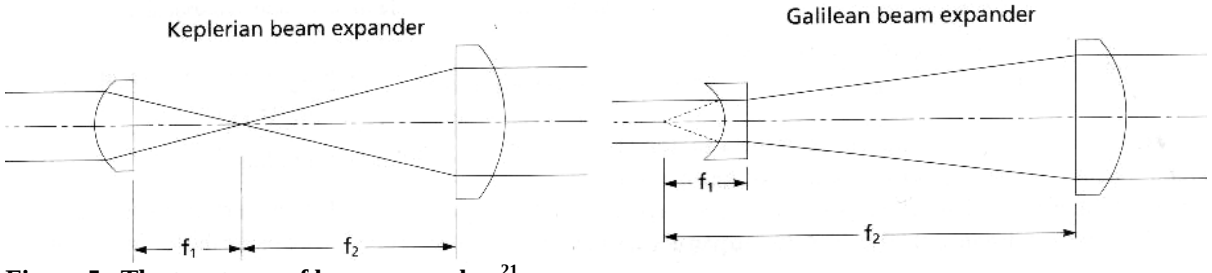

Figure 5. The two types of beam expanders[21].

Thus, a Melles Griot 25 LGR 173-230 green He-Ne laser, with λ = 543.5 nm and beam diameter = 0.79 mm was chosen, as any reduction in divergence would be advantageous and quickly offset a smaller initial beam diameter in

the far field. Also, green lasers have up to five times more visibility than red lasers with the same output power[22]. This facilitates aiming and pointing.

Even the selected laser, though, with a divergence θ_{FF} = 0.44 mrad, would produce a spot of 4.4 mm diameter at a distance z = 5 m. It was therefore advisable to further reduce the divergence by expanding and refocusing the beam, in order to produce a waist of bigger radius. This could be simply achieved by using two confocal lenses, either both converging (Keplerian beam expander) or one converging and the other diverging (Galilean beam expander), as shown in Fig. 5[21].

Using basic geometrical optics (see Fig. 5), the overall length of the optical system *OVL* is

$$OVL = f_1 + f_2 \tag{17}$$

and the magnification *MAG* is

$$MAG = \frac{f_2}{f_1} \tag{18}$$

where f_1 and f_2 are the focal lengths of the two lenses.

The behavior of a Gaussian beam can be significantly different from that which would be anticipated on the basis of simple geometrical optics, especially when, as in our case, a lens is placed in the near field of the incident beam. As in the work described in Ref. 20, the optimal set-ups can be found by a combination of empirical adjustment and attention to the less familiar aspects of Gaussian beam optics[21,23]. For the sake of simplicity and ease of operation, a commercial (Melles Griot) beam expander was employed, which turned out to be both a time and cost-effective solution.

C. The Position Sensitive Detector (PSD)

The basic principle of operation of the PSD is straightforward, as illustrated in Figs. 6 and 7[24]. When the laser light spot strikes the detector, an electric charge proportional to the light intensity is generated at the incident position. As the active area is also a resistive layer, this electric charge is driven through it and collected by the output electrodes as photocurrents, while being divided in inverse proportion to the distance between the incident position and each electrode. The use of four electrodes, as shown in Fig. 7 for a pin-cushion (improved tetra-lateral) type PSD, allows a two-

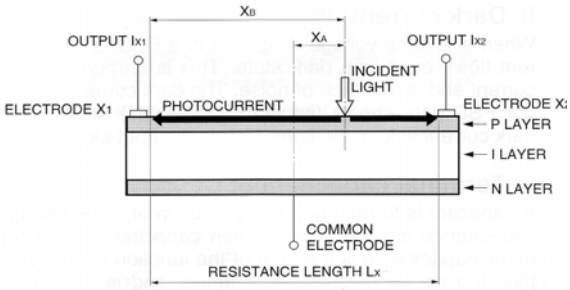

Figure 6. PSD sectional view[24].

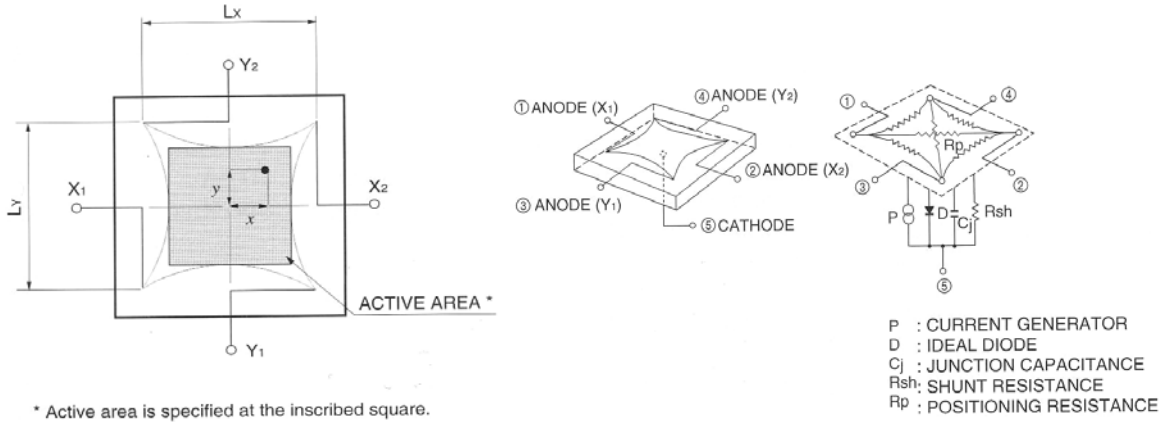

Figure 7. Active area and structure chart, with equivalent circuit[24].

dimensional displacement measurement[24].

The introduction of the PSD was a marked improvement of the measurement system described in Ref. 20 with respect to the set-up used in Ref. 25, where the laser displacement was read visually on a screen through a scale with a 0.5 mm resolution.

III. Experimental Apparatus

The development of the thrust balance was planned to be carried out in two phases. In the first one the thrust measurement is analyzed and a calibration procedure set up using an initial prototype in atmospheric environment. In the second one a final model is built, calibrated outside the vacuum chamber and then installed in its interior for a final calibration and following in-situ thrust measurements of ion thrusters.

D. Hardware

The initial prototype, which is in the final stage of characterization, consists of a series of 7 galvanized steel AISI 1020 rings (seizing 50-cm external diameter, 40-cm internal diameter and 0.5-mm thickness), a galvanized steel AISI 1020 centre plate, which supports the setup as whole, and a stainless steel AISI 304 conical target, as shown schematically in Fig.8 and assembled on the support used for the calibration outside the vacuum chamber in Fig. 9 (two different views). This prototype weights about 10 kg. Note the lower counterweight, by moving which we can vary the PTB equilibrium position, and the upper counterweight, the movement of which varies the position of the PTB center of gravity. The vertical position of the knife-edge suspensions is also adjustable. In this way, we can easily vary the distance R and therefore the sensitivity of our PTB (see Eq. 5). The final model of the thrust balance is under construction and all of its materials were substituted aiming to decrease its weight and to better withstand ion bombardment. This model will have the same dimensions as the calibration model and it will be built using aluminum alloy 2024 for the intermediate disks, TiAl6V4 for both the front disk and centre plate, and graphite R7510 for the conical target. This latter will present a double-conical shape, with semiangles of 30ºand 45º (see Fig. 10), selected after extensive simulations of particle impacts on the target. Such simulations, where the impinging particles were modeled as hard spheres undergoing quasi-elastic collisions, aimed at minimizing the amount of particles bouncing back with appreciable axial momentum. A frame from a movie, realized with 3D Studio Max, is shown in Fig. 11. The disc at the top, emitting a beam of particles with a 15º divergence, simulates the ion thruster.

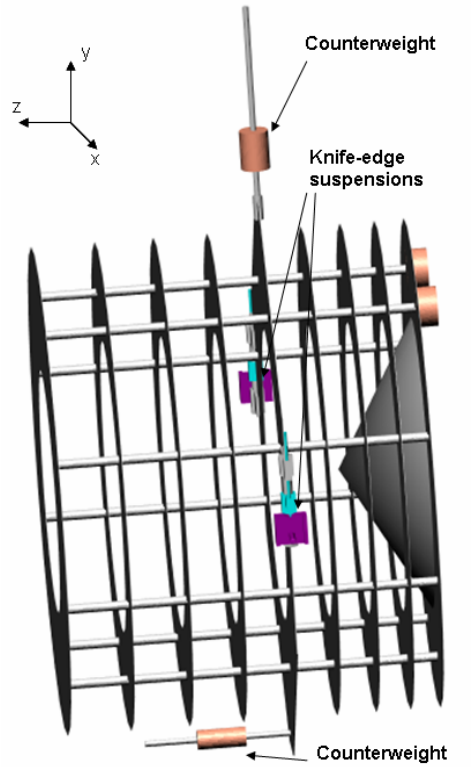

Figure 8. PTB initial prototype schematic.

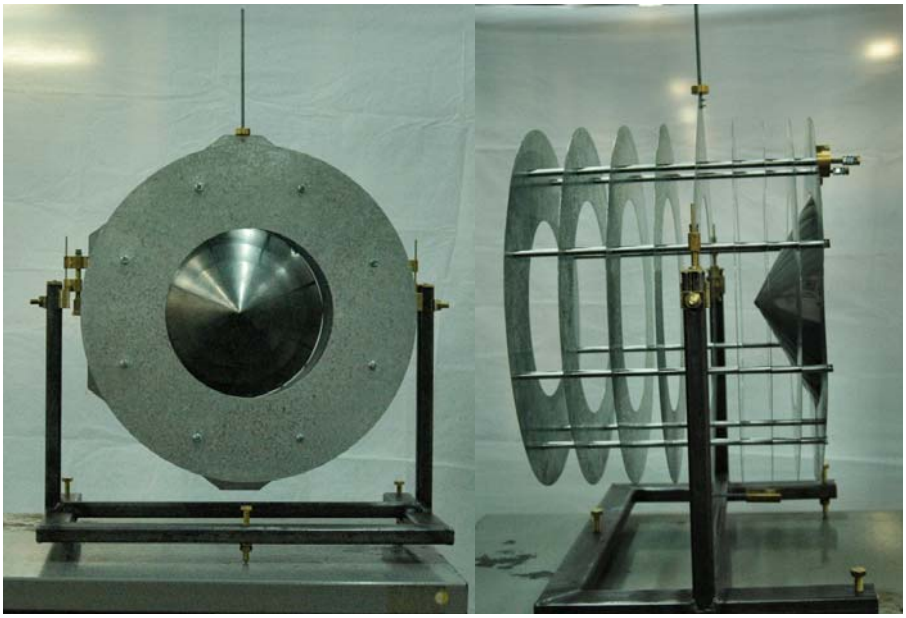

Figure 9. PTB initial prototype front (left) and side wiews.

Both models of balance share the same equipment used for the LOL: a Melles Griot 25 LGR 173-230 HeNe laser, with λ = 543.5 nm and 0.8 mW power, and a Hamamatsu S1881 PSD with a C9069 signal processing circuit. The S1881 model, with an Active Surface Area (ASA) of nearly 500 mm^2, over twenty times as large as the S2044 one used in Ref. 20, can measure values of Δx up to 22 mm. This sensor allows us to measure the displacement of the laser beam on its surface with a maximum resolution, in optimal operating conditions (strong and well-centered signal), of 6.35 μm[26], which then dictates the maximum thrust measurement resolution. This could be improved, as shown by Eqs. 3.2 and 3.3, by increasing the optical path P. But, if the optical path P needs to be quite long, as in the present case when measuring thrusts in large vacuum chambers, and PSDs with large ASAs are needed, a limit is soon reached. Larger PSDs can measure larger values of Δx but, as the smallest displacement that can be resolved is proportional to the sensor size, the total measurement resolution cannot be improved beyond a certain value. The optimal set-up is when the size of the PSD ASA is slightly larger than the maximum expected values of Δx, in order to make full use of the sensor while avoiding errors due to the laser spot falling partially outside of the ASA.

A narrow-bandpass interference filter with a transmission curve centered at the laser frequency, placed in front of the PSD, cuts off stray ambient light, which would interfere with the measurement. As the peak transmittance is still about 50%, a neutral density filter (ND = 1) is also needed, in order to decrease the incident light intensity and to avoid saturating the sensor.

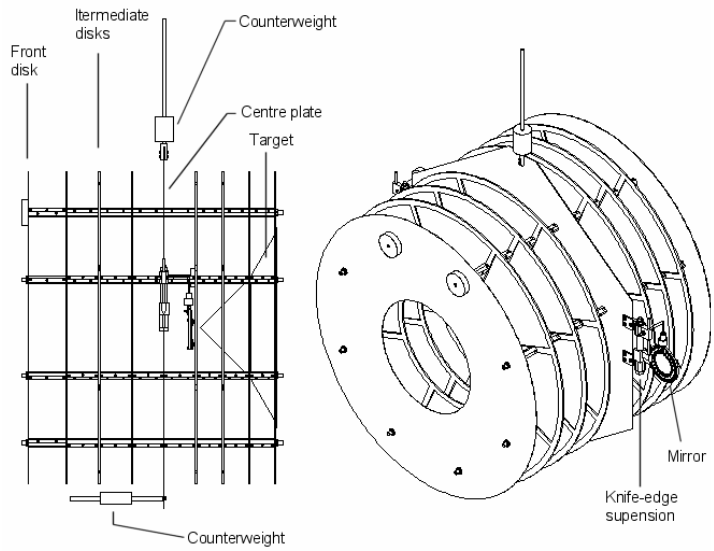

Figure 10. PTB final design schematic.

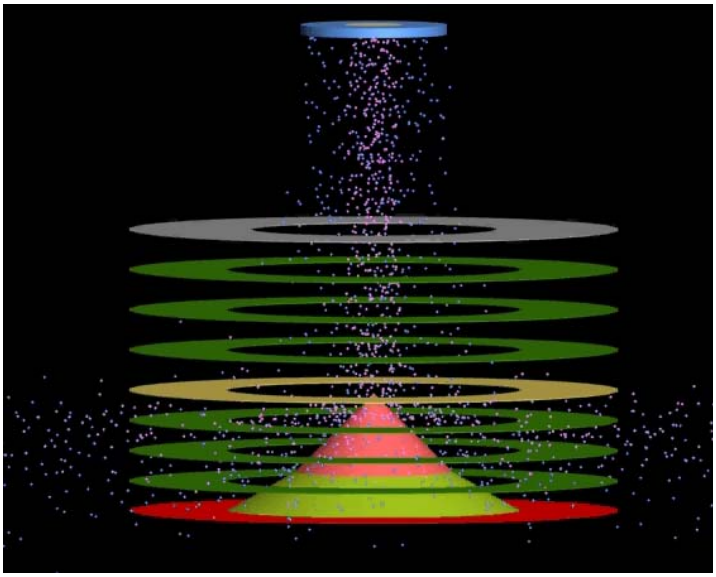

Figure 11. Simulation of particle impingement on the PTB.

E. Calibration

The initial prototype has been calibrated outside the vacuum chamber by means of masses, as described in Section II-A. These calibration masses were manufactured out of copper wire and their weight was accurately measured with a precision balance, resulting in a series of small hooks weighting 68±0.5 mg each. These were hanged at a precisely defined position on a small screwthread calibration arm fastened to the lower counterweight arm. The resulting moment caused the PTB to rotate. Due to the low damping coefficient of our system, weights were added and taken off at ten-minute intervals, to give the system time to stabilize and to have a long enough window to time-average the signal. The PTB was placed in front of the optical table where the laser, the beam expander, the filters and the PSD were mounted, as shown in Fig. 12. The laser beam was reflected off a mirror mounted on the PTB, clearly visible in the photo. The distance between this mirror and the PSD, equal to the optical path P, was accurately measured at each calibration run, and kept at approximately 2 m, close to what it will actually be in the final set-up with the PTB mounted inside the vacuum chamber (see Fig. 13).

Measurements were taken with the upper counterweight at its lowest and highest possible positions, which varied the PTB sensitivity slightly, but without varying the position of the knife-edge suspension axis. Time-averaged measurements are compared to theoretical simulations in Visual Nastran Desktop in Fig. 14. We can see that the simulations slightly overestimate the actual sensitivity, but the agreement is quite good, considering that the Nastran model is not identical to the actual prototype that was built, which underwent some slight modifications, and does not take into account friction at a "real" knife edge suspension. Such suspension, built out of brass in the initial prototype, will be manufactured out of hard steel in the final model. Considerable data scatter can be observed in Fig. 14, largely due to variations between experimental runs taken on different days, after the whole assembly had been moved around the Laboratory to allow other activities to be carried out. Also note that the data shown in Fig. 14 were collected before the beam expander became available. With this latter, it is possible to obtain a much smaller (~1 mm) laser beam diameter at the PSD.

From Eq. (10), we can calculate for our prototype PTB a sensitivity of 45 μN/μrad, which, with P = 2 m, translates into 11 μN/μm, from Eq. (13). This means that, in optimal PSD operating conditions, already our prototype measurement system could resolve thrusts down to 70 μN. While this does not seem impressive at first sight, it is to be remembered that this calibration was carried out more for the sake of establishing a procedure than to optimize the system performance. During the calibration of the PTB final model, adjustments will be made of the position of the knife-edge suspensions and of the center of gravity, in order to bring the sensitivity down into the μN range.

Figure 12. Prototype PTB calibration set-up.

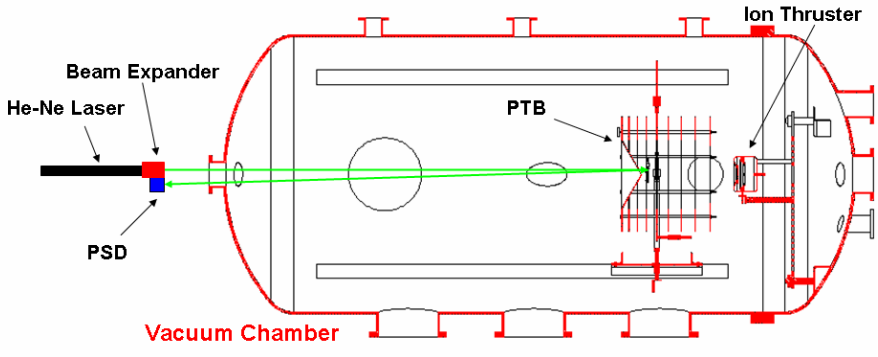

Figure 13. Final PTB set-up inside the vacuum chamber.

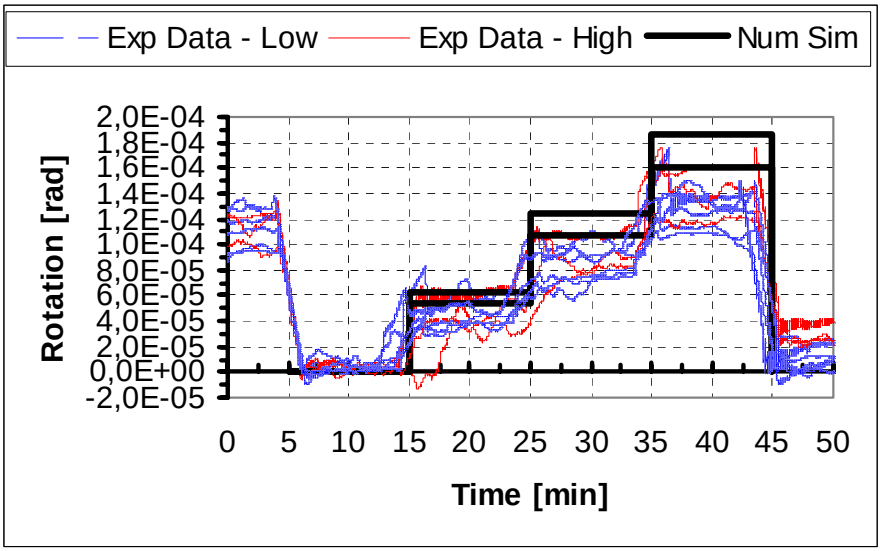

Figure 14. Prototype PTB calibration results, compared with numerical simulations.

IV. Conclusion

A thrust measurement system, based on a Pendulum Target Balance (PTB), is being built in order to evaluate the performance of the ion thrusters developed in the EP laboratory at the Associated Plasma Laboratory (LAP) of the National Institute for Space Research (INPE) in São José dos Campos, SP, Brazil. An initial prototype has already been calibrated with results in good agreement with numerical predictions. The final model is being assembled and will be calibrated first outside and then inside the vacuum chamber, to be later used for actual ion engine thrust measurements.

Acknowledgments

The authors wish to thank FAPESP, the State of São Paulo Research Foundation, for funding this project.

References

[1]Burton, R. L. and Turchi, P. J., "Pulsed Plasma Thruster", *Journal of Propulsion and Power*, Vol. 14, No. 5, 1998, pp. 716-735.

[2]Choueiri, E. Y., "System Optimization of Ablative Pulsed Plasma Thruster for Stationkeeping", *Journal of Spacecraft and Rockets*, Vol. 33, No. 1, 1996, pp. 96-100.

[3]Yang, T. F., Liu, P., Chang-Diaz, F. R., Lander, H., Childs, R. A., Becker, H. D. and Fairfax, S. A., "A Double Pendulum Plasma Thrust Balance and Thrust Measurement at a Tandem Mirror Exhaust," *Review of Scientific Instruments*, Vol. 66, 1995, pp. 4637-4643.

[4]Paccani, G. and Ravignani, R., "Sulla Misura Indiretta della Spinta di Propulsori Elettrici," *Aerotecnica Missili e Spazio*, Vol. 74, 1995, pp. 103-110.

[5]Chavers, D. G., Chang-Diaz, F. R., Irvine, C. and Squire, J. P., "Momentum and Heat Flux Measurements in the Exhaust of VASIMR Using Helium Propellant," *28th International Electric Propulsion Conference,* IEPC Paper 03-028, 2003.

[6]Gruber, J. R., "Low-Energy Sputter Erosion of Various Materials in a T5 Ion Thruster," *27th International Electric Propulsion Conference,* IEPC Paper 01-307, 2001.

[7]Matsunami, N., Yamamura, Y., Itoh, N., Tawara, H. and Kawamura, T., "Energy Dependence of Ion-Induced Sputtering Yields of Monoatomic Solids in the Low Energy Region," Nagoya Institute of Plasma Physics IPPJ-AM-52, 1987.

[8]Yamamura, Y. and Tawara, H., "Energy Dependence of Ion-Induced Sputtering Yields from Monoatomic Solids at Normal Incidence," *Atomic Data and Nuclear Data Tables*, Vol. 62, 1996, pp. 149-253.

[9]Cercignani, C. and Lampis, M., "Free Molecular Flow Past a Flat Plate in the Presence of a Nontrivial Gas-Surface Interaction," *Journal of Applied Mathematics and Physics*, Vol. 23, 1972, pp. 713-728.

[10]Woronowicz, M. S. and Rault, D. F. G., "Cercignani-Lampis-Lord Gas-Surface Interaction Model: Comparisons Between Theory and Simulation," *Journal of Spacecraft and Rockets*, Vol. 31, 1994, pp. 532-534.

[11]Bird, G. A., *Molecular Gas Dynamics and the Direct Simulation of Gas Flows*: Oxford University Press, 1994.

[12]Lord, R. G., "Some Extensions to the Cercignani-Lampis Scattering Kernel," *Physics of Fluids A: Fluid Dynamics*, Vol. 3, 1991, pp. 706-710.

[13]Longden, A. C., "On the Irregularities of Motion of the Foucault Pendulum", *Physical Review*, Vol. 13, No. 4, 1919, pp. 241-258.

[14]Levi-Civita, T. and Amaldi, U., *Lezioni di Meccanica Razionale*: Zanichelli Ed., 1923.

[15]Kimura, I., Yanagi, R. and Inoue, S., "Preliminary Experiments on Pulsed Plasma Thrusters with Applied Magnetic Fields", *AIAA/DGLR 13th International Electric Propulsion Conference*, AIAA Paper 78-655, 1978.

[16]Yanagi, R. and Kimura, I., "A New Type Target for the Measurement of Impulse Bits of Pulsed Plasma Thrusters", *15th International Electric Propulsion Conference*, AIAA Paper 81-0712, 1981.

[17]Gessini, P. and Paccani, G., "Ablative Pulsed Plasma Thruster System Optimization for Microsatellites", *27th International Electric Propulsion Conference*, IEPC Paper 01-182, 2001 and References therein.

[18]Gessini, P., Intini Marques, R., Gabriel, S. B. and Veres, S. M., "Propulsion System Optimisation for Satellite Formation Flying, *4th International Workshop on Satellite Constellations and Formation Flying*, 2004 and References therein.

[19]Kameoka, M., Takegahara, H., Shimizu, Y. and Toki, K., "Single Impulse Measurement of a Coaxial Pulsed Plasma Thruster", *28th International Electric Propulsion Conference*, IEPC Paper 03-093, 2003.

[20]Gessini, P., "Measurement of the Thrust Generated by a Hollow Cathode with Noble Gases," Ph.D. Dissertation, Aerospace Engineering Department, University of Southampton, Southampton, UK, 2006.

[21]Anonymous, "Gaussian Beam Optics", in *Melles Griot Cat*., 1997.

[22]Anonymous, "Helium Neon Lasers", in *Melles Griot Cat*., 1997.

[23]Self, S. A., "Focusing of Spherical Gaussian Beams", *Applied Optics*, Vol. 22, 1983, pp. 658-661.

[24]Anonymous, *Hamamatsu Cat*. No. KPSD0001E01, 2002.

[25]Gessini, P., Gabriel, S. B., and Fearn, D. G., "Hollow Cathode Thrust Measurements Using a Target: Initial Results and Some Issues," *28th International Electric Propulsion Conference,* IEPC Paper 03-253, 2003 and References therein.

[26]Anonymous, *Hamamatsu Op. Man*. DWG. No. K32-B60025, 2005.